Environmental Science & Technology

pubs.acs.org/est

Article

Fe^{2+}/HClO Reaction Produces $Fe^{IV}O^{2+}$: An Enhanced Advanced Oxidation Process

Sheng Liang, Liuyi Zhu, Jian Hua, Weijian Duan, Puu-Tai Yang, Shan-Li Wang, Chaohai Wei, Chengshuai Liu,* and Chunhua Feng*

Cite This: *Environ. Sci. Technol.* 2020, 54, 6406−6414

Read Online

ACCESS | Metrics & More | Article Recommendations | Supporting Information

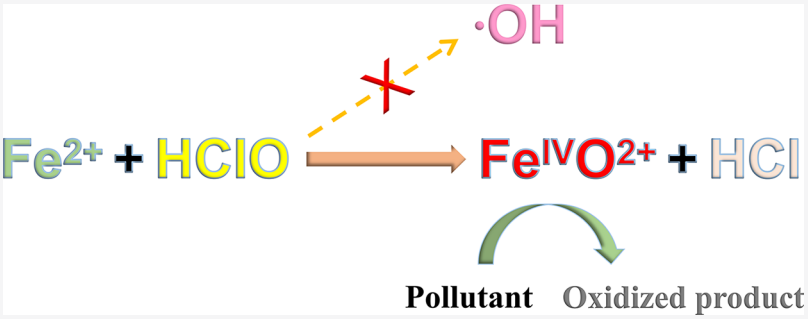

ABSTRACT: The reaction between Fe^{2+} and HClO constitutes a promising advanced oxidation process (AOP) for removing pollutants from wastewater, and •OH has been considered the dominant reactive oxidant despite limited evidence for this. Herein, we demonstrate that the Fe^{2+}/HClO reaction enables the production of $Fe^{IV}O^{2+}$ rather than •OH in acid medium, a finding that is strongly supported by multiple lines of evidence. Both X-ray absorption near-edge structure spectroscopic tests and Mössbauer spectroscopic tests confirmed the appearance of $Fe^{IV}O^{2+}$ as the reactive intermediate in the reaction between Fe^{2+} and HClO. The determination of $Fe^{IV}O^{2+}$ generation was also derived from the methyl phenyl sulfoxide (PMSO)-based probe experiments with respect to the formation of $PMSO_2$ without •OH adducts and the density functional theory studies according to the lower energy barrier for producing $Fe^{IV}O^{2+}$ compared with •OH. A dual-anode electrolytic system was established for the in situ generation of Fe^{2+} and HClO that allows the production of $Fe^{IV}O^{2+}$. The system exhibits an enhanced capacity for oxidizing a model pollutant (e.g., phosphite) from industrial wastewater, making it an attractive and promising AOP for the abatement of aqueous contaminants.

INTRODUCTION

The reaction between Fe(II) and H_2O_2 for generating strong oxidants has had numerous industrial and environmental applications since its discovery in 1894 by the British chemist H.J.H. Fenton. (The reaction was accordingly named after him.)[1] The Fenton reaction generates intermediates showing a powerful capability to oxidize a wide variety of inorganic and organic pollutants, which is an important step in iron-based advanced oxidation processes (AOPs) for the abatement of contaminants in wastewater and soil.[2,3] Despite extensive efforts to identify the key oxidative intermediate species, a fundamental question has been the object of decades of debate:[3] whether the main oxidant is •OH generated via the Haber−Weiss pathway (i.e., homolytic O−O bond cleavage)[4] or Fe(IV) formed through the Bray−Gorin pathway (i.e., heterolytic O−O bond cleavage).[5] So far, the consensus on this traditional Fenton reaction is that •OH is the dominant species produced in an acid medium (pH < 6), whereas Fe(IV) is the dominant species generated under a near-neutral medium (pH > 6).[6] Recently, this kind of disputation has also been extended to some analogous Fenton-like reactions, in which H_2O_2 is replaced by O−O-contained substances, such as peroxydisulfate,[7] peroxymonosulfate,[8] and peracetic acid.[9] Indeed, the production of Fe(IV), instead of reactive radicals (e.g., •OH), in the iron redox system has attracted much attention in the field of advanced oxidation[10] because Fe(IV) is capable of allowing selective oxidation and •OH engages in uncontrolled oxidation.[8,11]

In addition to the peroxide compound, the substitution of H_2O_2 by HClO to create stronger oxidants for eliminating contaminants in the iron redox system has also attracted attention in the field of advanced oxidation.[12] In acid medium, the application of the reaction between Fe^{2+} and HClO as an emerging AOP can be accomplished in an electrochemical system, integrating Fe^{3+}/Fe^{2+} recycled at the cathode and

Received: January 12, 2020
Revised: March 9, 2020
Accepted: March 11, 2020
Published: March 11, 2020

https://dx.doi.org/10.1021/acs.est.0c00218
Environ. Sci. Technol. 2020, 54, 6406−6414

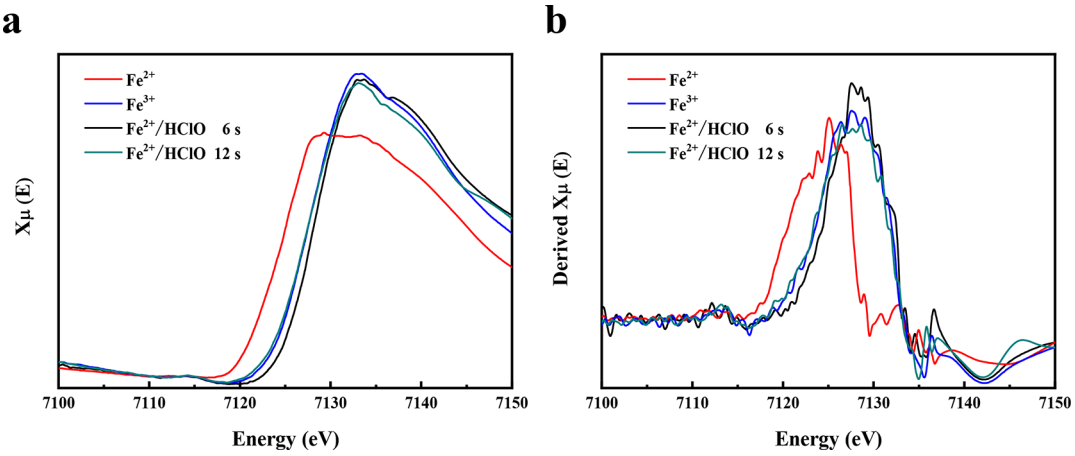

Figure 1. Normalized XANES spectra of Fe^{2+}, Fe^{3+}, and Fe^{2+}/HClO samples: (a) normalized spectra in Xμ/energy and (b) normalized spectra in the derived Xμ/energy. [Fe^{2+}] = [HClO] = 0.5 mM and pH = 2.0.

chlorine-based electro-oxidation (EO) at the anode (eqs 1&2).[13] Several previous studies in the literature[12−14] have demonstrated that the electrogenerated Fe^{2+}/HClO-involved AOP is effective in abating organic pollutants from aqueous solutions and proposed the possibility of $^{\bullet}OH$ formation that is attributed to HClO activation by Fe^{2+}, a reaction (eq 3) analogous to the H_2O_2 reaction with Fe(II). However, no convincing evidence for the occurrence of $^{\bullet}OH$ has been presented, and the possibility of $Fe^{IV}O^{2+}$ (an abbreviation of $[Fe^{IV}{=}O]^{2+}$) generation via (eq 4) should be considered.[15,16] It remains unknown whether $^{\bullet}OH$ or $Fe^{IV}O^{2+}$ is the dominant reactive oxidant produced from the reaction between HClO and Fe^{2+}, which may impede the broad application of this AOP; as such, it has stimulated our great interest in distinguishing $Fe^{IV}O^{2+}$ and $^{\bullet}OH$ produced in the HClO-participating Fenton-like reaction. To unravel an ambiguous mechanism, compelling evidence, especially direct evidence, must be provided. It has been suggested that various spectroscopic techniques show solid evidence to support the generation of Fe(IV)−oxo species from the reaction of Fe(II) complexes with an oxygen atom donor such as *m*-chloroperbenzoic acid, iodosylbenzene (PhIO), or O_3 via heterolytic O−O bond cleavage.[17−20]

$$2Cl^- \rightarrow Cl_2 + 2e^- \quad (1)$$

$$Cl_2 + H_2O \rightarrow HClO + HCl \quad (2)$$

$$Fe^{2+} + HClO \rightarrow Fe^{3+} + {}^{\bullet}OH + Cl^- \quad (3)$$

$$Fe^{2+} + HClO \rightarrow Fe^{IV}O^{2+} + HCl \quad (4)$$

Herein, we identify for the first time the HClO-stimulated two-electron transformation of Fe^{2+} to $Fe^{IV}O^{2+}$ rather than $^{\bullet}OH$ generation in acidic solution and provide multiple instances of solid evidence by characterizing it in experimental and theoretical aspects. These include Fe K-edge X-ray absorption near-edge structure (XANES) spectroscopic characterizations, Mössbauer spectroscopic tests, methyl phenyl sulfoxide (PMSO)-based probe experiments, electron spin resonance (ESR) characterizations, quenching experiments, and thermodynamic density functional theory (DFT) calculation studies. To test the enhancement of pollutant oxidation with $Fe^{IV}O^{2+}$ from a Fe^{2+}/HClO reaction, a dual-anode electrochemical system was set up for in situ generation of Fe^{2+} and HClO from an Fe anode and a mixed metal oxide (MMO) anode, respectively, in an acid medium containing Cl^-, followed by the assessment of its performance for the oxidation of phosphite, which is a stubborn eutrophication contaminant that requires advanced oxidation treatment. Our previous work has shown that a preoxidation process is an essential prerequisite for the sufficient removal of phosphite by coagulation in phosphite-laden wastewater.[21]

EXPERIMENTAL SECTION

Chemicals and Electrode Materials. 5,5-Dimethyl-1-pyrroline N-oxide (DMPO, purity > 97%), PMSO (purity > 99%), methyl phenyl sulfone ($PMSO_2$, purity > 99%), dimethyl sulfoxide (DMSO, purity > 99%), tertiary butanol (TBA), $Fe(ClO_4)_3{\cdot}H_2O$, $Fe(ClO_4)_2$ (purity > 98%), iron powder (purity > 99%), and sodium phosphite ($Na_2HPO_3{\cdot}5H_2O$) were purchased from Sigma-Aldrich (St. Louis, MO, USA). $NaClO{\cdot}5H_2O$ (available chlorine min. 40.0%) was purchased from TCI (Shanghai) Development Co., Ltd. All other chemicals, being of at least analytical grade, were utilized as received without further purification. For in situ generation of Fe^{2+} and HClO, an electrochemical reactor was constructed with an MMO anode (IrO_2−RuO_2-type coated titanium plate, Changli Specialty Metals Ltd., Shanxi, China), an Fe plate anode (DT-3 type, Rui Yuan Armco-iron Co., Ltd., Jiangsu, China), and a stainless steel plate cathode (304 type, Zhong Run Hongfa Stainless Steel Co., Ltd., Shenzhen, China).

Spectroscopic, Chemical, and Theoretical Characterizations on the Product of Fe^{2+}/HClO Reaction. The XANES spectra were collected at beamline 44A of the Taiwan Photon Source synchrotron facility. The Mössbauer spectra were measured using an automated precision Mössbauer spectrometric system with a high-velocity resolution (registration in 1024 channels) built on the basis of a Mössbauer spectrometer WSS-10 (WissEl GmbH, Germany). The electrospray ionization-triple quadrupole mass spectrometry (ESI-QqQMS) measurements were performed using an AB SciexAPI 4000^+ QqQMS analysis system (AB Sciex, Toronto, Canada) with an ESI source. The ESR experiments were performed using a spectrometer (EMX-10/12, Bruker, Karlsruhe, Germany). DFT calculations were performed using the Gaussian 09 quantum chemistry software package. More details on these measurements are documented in the Supporting Information (Section S1−S4).

https://dx.doi.org/10.1021/acs.est.0c00218
Environ. Sci. Technol. 2020, 54, 6406−6414

In Situ Generation of Fe^{2+} and HClO in a Dual-Anode Electrolytic Cell and Its Application in the Acceleration of Phosphite Oxidation. Batch experiments for the in situ formation of Fe^{2+} and HClO were conducted in an undivided electrolytic cell at an initial pH of 2.2, which contains an MMO anode, an Fe plate anode, and a stainless steel plate cathode, each having a size of 3 cm × 3 cm. The application of this system for phosphite oxidation was evaluated by detecting the phosphate generation as a function of electrolysis time. The detailed experimental procedures are presented in the Supporting Information (Section S5).

RESULTS AND DISCUSSION

Identification of $Fe^{IV}O^{2+}$ Produced from the Fe^{2+}/HClO Reaction Using XANES and Mössbauer Spectra. To monitor the valence variation of Fe during the process of Fe^{2+}/HClO reaction, XANES in a fluorescent mode was carried out on four related samples, including pure Fe^{2+} solution, pure Fe^{3+} solution, and Fe^{2+}/HClO mixture at 6 s and 12 s, all frozen with liquid nitrogen before the characterizations (see the detailed procedures in Section S1). As shown in Figure 1, the edge energies of these samples were revealed and compared with each other, as they provide information about the valent states of Fe. The peak energy shifted from 7124 eV of the pure Fe^{2+} sample to near 7129 eV of the Fe^{2+}/HClO mixture (mixed over 6 s) and shifted back to 7128 eV of the Fe^{2+}/HClO mixture (mixed over 12 s), which was approximately equivalent to that of the pure Fe^{3+} sample. The K-edge energy shift to higher values is closely linked to the increase in the Fe valence state, the positive shift by 3.5−4 eV corresponding to the valence state change by +1.[22,23] The nearly 1 eV of the right shift of Fe^{2+}/HClO compared with Fe^{3+} indicated an average Fe valence of approximately +3.25 for the resulting species after 6 s, which clearly indicates that a ferryl species (at a valence higher than +3) should be generated during the rapid reaction between Fe^{2+} and HClO.[24] The back shift for the edge energy of the Fe^{2+}/HClO mixture to 7128 eV after 12 s reflected that the ferryl species (most likely attributed to $Fe^{IV}O^{2+}$ because of the two-electron transfer character of HClO)[25] is a fairly reactive intermediate[26] whose life span is so short that the majority of all Fe species in the Fe^{2+}/HClO mixture might end up at Fe^{3+}.[20] This is due to the quenching of ferryl species such as $Fe^{IV}O^{2+}$subject to reduction by Fe^{2+} and its self-decomposition to Fe^{3+} according to the literature.[20,27]

To clearly recognize and identify the ferryl species generated from the Fe^{2+}/HClO reaction, the corresponding Mössbauer spectra of the $^{57}Fe^{2+}$/HClO mixture were recorded (see the detailed procedures in Section S1), as presented in Figure 2. The Mössbauer spectrum of $^{57}Fe^{2+}$ without HClO exhibits a doublet with an isomer shift (δ) of 1.37 mm s^{-1} and a quadrupole splitting (Δ) of 3.27 mm s^{-1}, which are typical characteristics of a high-spin Fe(II) species.[28] The resultant Mössbauer spectrum of the $^{57}Fe^{2+}$/HClO sample mixed for 6 s can be analyzed as a superposition of the spectrum of Fe(II) (60.4% of total intensity, blue line)[29] and a new singlet (red line) with δ = −0.26 mm s^{-1}, which is consistent with the assignment of this "oxidized Fe" species as Fe(IV) by Chen et al.[30] No clear signal of Fe(III) was observed in this sample; this might be attributable to the small percentage of Fe(III) generated within the short period of 6 s. Fe(IV) has four 3d electrons, and the paramagnetic states of Fe(IV) have spins of either S = 2 or S = 1.[31] The parameters obtained in the present

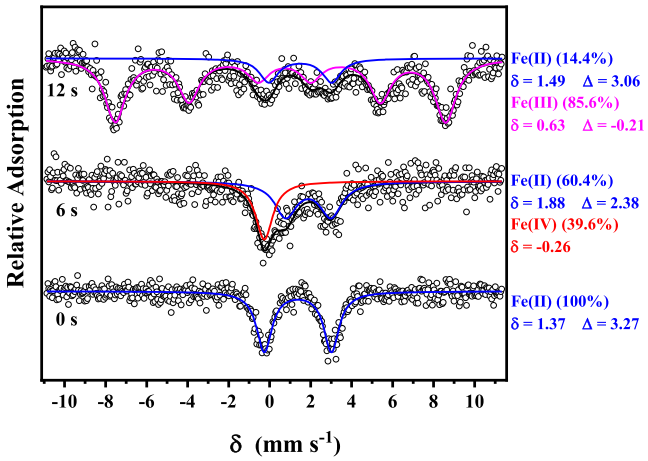

Figure 2. Mössbauer spectra of $^{57}Fe^{2+}$ and $^{57}Fe^{2+}$/HClO samples (mixed for 6 s and after 12 s). $[Fe^{2+}]$ = [HClO] = 0.5 mM and pH = 2.0. The spectra were collected at 12 K in transmission mode with a WSS-10 Mössbauer spectrometer equipped with a closed-cycle cryostat. The spectra were calibrated against 7 μm α-Fe^0 foil and fit using MossWinn software.

study are similar to those of S = 2 Fe(IV).[32] Most plausibly, the Fe(IV) species is formulated as $[Fe^{IV}{=}O(H_2O)_5]^{2+}$.[20] The larger isomer shift observed for S = 2 $Fe^{IV}O^{2+}$ (δ = −0.26 mm s^{-1}) is not a consequence of the unusual trigonal bipyramidal coordination geometry but rather an intrinsic property of the S = 2 state as it necessarily populates a strongly antibonding orbital, which gives rise to significant metal−ligand bond elongations.[33] The spectrum of the $^{57}Fe^{2+}$/HClO sample collected after 12 s of mixing delivers a major high-spin Fe(III) species of sextuplet (pink line), with parameters (δ = 0.63, Δ = −0.21) similar to those reported for Fe^{3+} in the literature.[20] This accords with the XANES data showing that, after an extended period of time, the predominant Fe species is Fe^{3+} because of the short τ of reactive $Fe^{IV}O^{2+}$ in acid solution.[34]

Evidence of $Fe^{IV}O^{2+}$ Generation through PMSO-Based Probe Experiments Using Mass Spectra. Previous studies on $Fe^{IV}O^{2+}$ generation in AOPs have shown that the differentiation between $Fe^{IV}O^{2+}$ and radicals (e.g., $^{\bullet}OH$ and $SO_4^{\bullet-}$) can be attained with a sulfoxide such as PMSO or DMSO as a probe.[7] This is because sulfoxide oxidation by $Fe^{IV}O^{2+}$ is subjected to oxygen atom transfer to form sulfone (e.g., $PMSO_2$ or $DMSO_2$), a product different from that generated upon the reaction between sulfoxide and $^{\bullet}OH$.[6,16,35] The reaction among Fe^{2+}, HClO, and PMSO was carried out in an acid medium (pH = 2.0) with a molar ratio of 2:2:1 (Fe^{2+}/HClO/PMSO), and the products were detected by ESI-QqQMS in the positive and full scan mode (see the detailed procedures in Section S2). For comparison, the typical Fenton reaction between Fe^{2+} and H_2O_2 under the same conditions was undertaken for the generation of $^{\bullet}OH$, and the oxidation of PMSO was also monitored. Figure S1 shows the positive ESI-QqQMS scans of pure PMSO and $PMSO_2$ chemicals, each exhibiting one intense peak appearing at m/z 141.0 and 157.2, respectively. As shown in Figure 3, in the Fe^{2+}/H_2O_2 system, the dominant spectrum appeared at m/z 158.1, indicating $^{\bullet}OH$-induced PMSO oxidation (Figure 3a). The product ion mass spectra of m/z 158.1 yielded peaks at 141.1, 143.1, 126.0, and 124.2, which should be the products of the cleavage of the methyl (15/CH_3) and hydroxyl (17/OH) groups (Figure 3c). Conversely, in the Fe^{2+}/HClO system (Figure 3b), the

https://dx.doi.org/10.1021/acs.est.0c00218
Environ. Sci. Technol. 2020, 54, 6406−6414

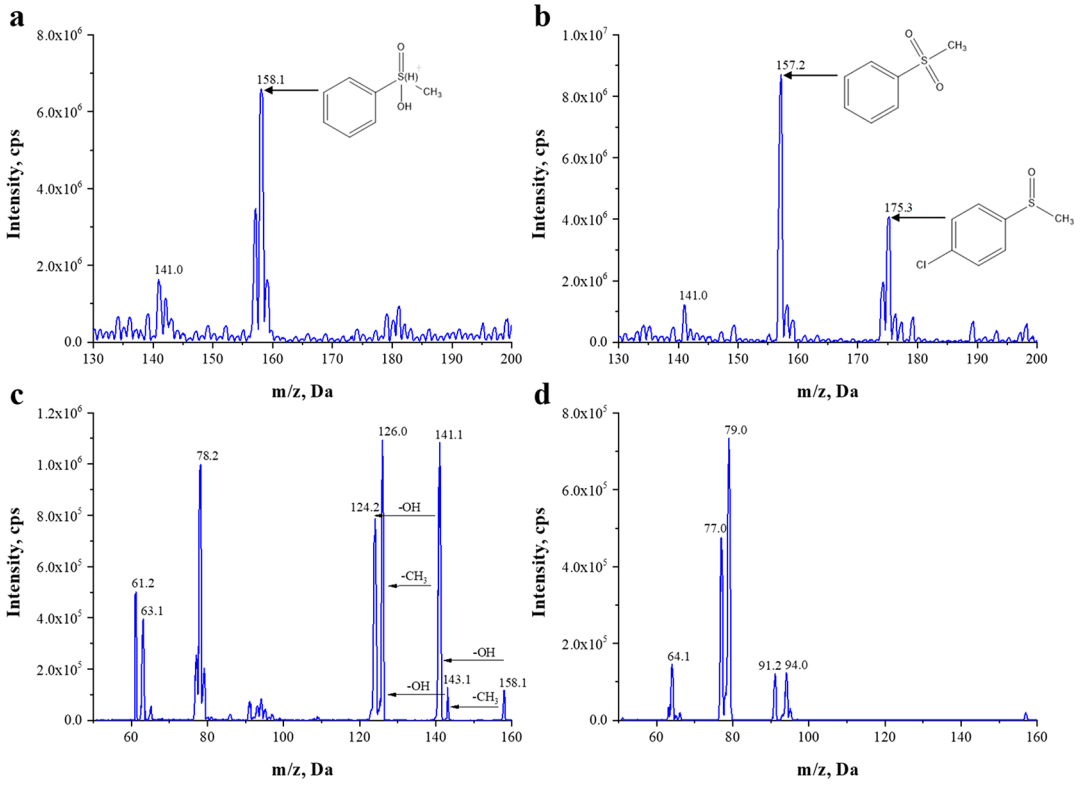

Figure 3. ESI-QqQMS of PMSO oxidation products (a,b) and the related product ion mass spectra (c,d) in the Fe^{2+}/H_2O_2 (a,c) and Fe^{2+}/HClO (b,d) systems. [PMSO] = 200 μM; [Fe^{2+}] = [H_2O_2] = [HClO] = 400 μM; reaction time = 20 min; and pH = 2.0.

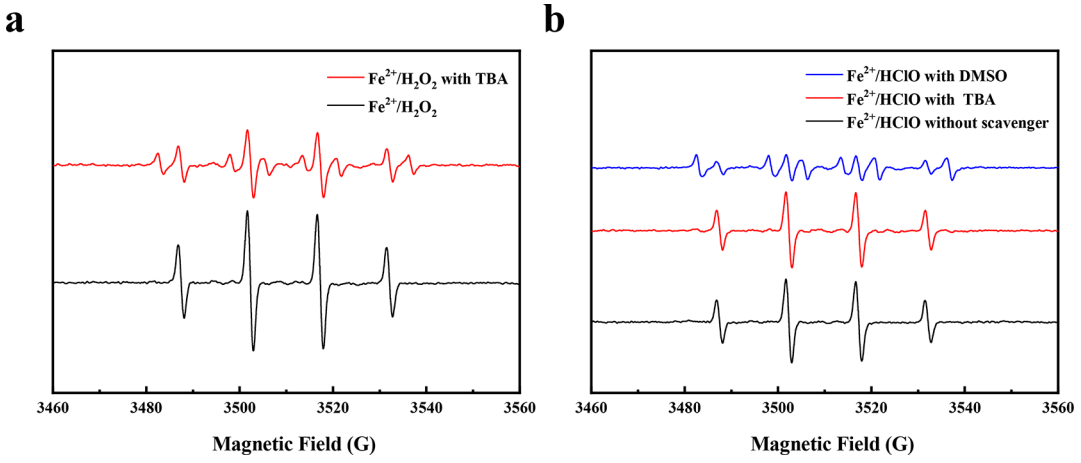

Figure 4. DMPO-probed ESR spectra of Fe^{2+}/H_2O_2 (a) and Fe^{2+}/HClO (b) with different scavengers. [Fe^{2+}] = 200 μM; [H_2O_2] = [HClO] = 400 μM; [DMSO] = [TBA] = 50 mM; [DMPO] = 100 mM; reaction time = 2 min; and pH = 2.0.

spectrum was dominated by a strong peak at m/z 157.2, which corresponds to the presence of $PMSO_2$, and a minor peak at m/z 175.3 that is attributable to the oxidation of PMSO directly by HClO (Figure S3). The product ion mass spectrum of m/z 157.2 (Figure 3d) was the same as that of the $PMSO_2$ standards (Figure S2), an indication of the absence of $^{\bullet}OH$ involvement. The formation of $PMSO_2$ and the absence of $^{\bullet}OH$ adducts of PMSO provided evidence for the generation of $Fe^{IV}O^{2+}$ in the Fe^{2+}/HClO system, highly concomitant with $PMSO_2/DMSO_2$ formation from PMSO/DMSO oxidation attributed to $Fe^{IV}O^{2+}$ generated in processes such as Fe^{2+}/O_3,[20] Fe(II)/peroxydisulfate,[7] and Fe(III)-tetraamidomacrocyclic/peroxymonosulfate[8] systems, as reported in recent years.

DMPO-Probed ESR Spectra Indicative of Nonradical Pathway in the Fe^{2+}/HClO Reaction. A series of ESR tests using DMPO as a spin-trapping agent were performed to identify and compare the reactive species generated from the Fe^{2+}/HClO and the reference Fe^{2+}/H_2O_2 systems in the presence and absence of scavengers (see the detailed procedures in Section S3). As shown in Figure 4, the ESR spectrum of Fe^{2+}/HClO exhibited a legible signal of DMPO−OH adducts (h_{fsc} of αN = αH = 14.9 G), which was exactly coincident with the ESR spectrum that resulted from Fe^{2+}/H_2O_2. This signal is generally assigned to the production of $^{\bullet}OH$.[36] Nevertheless, the DMPO−OH adducts generated could also be attributed to the production of $Fe^{IV}O^{2+}$.[7] Except for the adducts of DMPO scavenging free $^{\bullet}OH$,[37] the

https://dx.doi.org/10.1021/acs.est.0c00218
Environ. Sci. Technol. 2020, 54, 6406−6414

oxidation of DMPO by Fe(IV) also leads to the formation of DMPO−OH through a metal-catalyzed nucleophilic addition of water mechanism,[38] similar to the cases of high-valence Cu(III) and Mn(VII).[39] Despite the similarity of the ESR spectra for the two reactions, the utilization of different scavengers (e.g., DMSO and TBA) could distinguish the dominant reactive species based on the fact that Fe(IV) reacted with DMSO at a rate of 1.4×10^5 M^{-1} s^{-1}, 4 orders of magnitude higher than that (6.0×10^1 M^{-1} s^{-1}) of Fe(IV) with TBA in acid medium.[6,20] The DMPO−OH ESR signal of the Fe^{2+}/H_2O_2 system was distinctly suppressed upon the addition of TBA because TBA is a specific $^{\bullet}OH$ scavenger;[40,41] in contrast, the signal of the Fe^{2+}/HClO system changed insignificantly in the presence of TBA. On the other hand, the amendment of DMSO to the Fe^{2+}/HClO system caused a remarkable decline in the intensity of the DMPO−OH signal. These observations support that the oxidant generated in the Fe^{2+}/HClO system is different from the Fe^{2+}/H_2O_2 system in acid medium, which is ascribed to $Fe^{IV}O^{2+}$ instead of $^{\bullet}OH$.[27]

Because of the similarity in the structures of H_2O_2 and HClO (both contain the −OH group), it has been considered that the reaction between Fe^{2+} and HClO occurs in the same manner as that between Fe^{2+} and H_2O_2, and it is thus labeled a Fenton-like reaction, as proposed by Candeias et al. in 1994.[42] It was thought that the HClO molecule undergoes a one-electron activation by Fe^{2+} to produce $^{\bullet}OH$ and Cl^-,[43] analogous to the one-electron activation of H_2O_2 by Fe^{2+}. This radical-involved pathway may not occur in the case of HClO activation, as evidenced by a set of reference experiments in which a mild reducing agent (e.g., NH_3OHCl) was used to activate HClO or H_2O_2 in acid medium. As shown in Figure S4, distinct DMPO−OH ESR signals were visible as a consequence of one-electron activation of H_2O_2 by NH_3OHCl, whereas no ESR signals in relation to reactive radicals were displayed in the NH_3OHCl/HClO system. The possible reactions are listed as eqs S1 and S2. This phenomenon suggests the resistance of HClO activation to the production of $^{\bullet}OH$, which indirectly proves that the Fe^{2+}/HClO reaction proceeds via the nonradical pathway.

Thermodynamic DFT Calculations on the Fe^{2+}/HClO Reaction. DFT calculations of thermodynamics were performed to investigate the Fe^{2+}/HClO intermolecular reaction mechanisms using the Gaussian 09 quantum chemistry software package (see the detailed information in Section S4). To simulate the aquatic intermolecular reaction, 10 H_2O molecules were involved in the model, with six H_2O coordinated with Fe^{2+}.[44] The solvent effect (in water) was taken into account by the polarizable continuum model.[45] The relative energy of the intermediates and the barrier heights of all transition states in the reaction process were calculated (Figure 5). In the simulation model, $[Fe(H_2O)_6]^{2+}$ integrates with one HClO and four H_2O to form $[Fe(H_2O)_5(HClO)]^{2+}[(H_2O)_5]$ (**INT_1**). Then, **INT_1** undergoes a proton transfer to form $[Fe(H_2O)_5{-}OCl)]^{+}[(H_3O)^{+}][(H_2O)_4]$ (**INT_2**) via **TS_1** with a barrier height ($\Delta G^{\ddagger}_{298}$) of 10.7 kcal mol^{-1}. Finally, the O−Cl bond breaks via **TS_2** ($\Delta G^{\ddagger}_{298}$ = 16.9 kcal mol^{-1}) to release the chlorine anion, and Fe=O was formed to yield $[Fe{=}O(H_2O)_5]^{2+}$.[31] From the above, the total energy barrier of producing $[Fe{=}O(H_2O)_5]^{2+}$ and $[(H_3O)^{+}(H_2O)_4Cl^-]$ during the $[Fe(H_2O)_6]^{2+}$/HClO reaction is calculated to be 16.9 kcal mol^{-1}, which indicates that the entire transformation process could occur at room temperature with relatively rapid kinetics.[46] On the other hand,

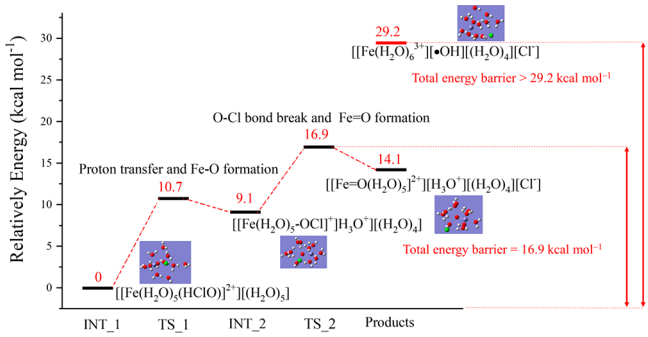

Figure 5. Energy profiles of the intermediates and the barrier heights of all transition states in the computational model for the $[Fe(H_2O)_6]^{2+}$/HClO reaction process.

the relative energy of the final product $[Fe(H_2O)_6]^{3+}[^{\bullet}OH]$-$[(H_2O)_4][Cl^-]$ was calculated and found to be 29.2 kcal mol^{-1} (~12 kcal mol^{-1} higher than the total energy barrier of producing $[Fe{=}O(H_2O)_5]^{2+}$ and $[(H_3O)^{+}(H_2O)_4Cl^-]$). This suggests that $[Fe{=}O(H_2O)_5]^{2+}$ is the reactive intermediate product during the $[Fe(H_2O)_6]^{2+}$/HClO reaction, whereas $^{\bullet}OH$ is unlikely to be produced during the process.[47]

Electrochemical Generation of Fe^{2+} and HClO for $Fe^{IV}O^{2+}$ Production and Its Role in Phosphite Oxidation. A scenario for the coexistence of Fe^{2+} and HClO can be attained in a dual-anode electrolytic cell, which is used for pollutant removal from Cl^--containing acid media, containing an Fe anode that dissolves into Fe^{2+} and an MMO anode that enables the anodic oxidation of Cl^- to produce HClO. We prove that the combination of in situ electrogenerated Fe^{2+} and HClO has a significantly enhanced capability of oxidizing pollutants. Phosphite was selected as the model pollutant as it is prevalent in acid electroless plating wastewater, and we have previously corroborated that a preoxidation process is necessary before it can be sufficiently removed from aqueous solution by coagulation.[21] Figure 6a,b shows and compares the time courses of phosphate (i.e., product of phosphite oxidation) concentrations, which are appreciably affected by the concentration of Cl^- and the in situ addition of Fe^{2+} (released from the Fe anode) in the presence of Cl^- in the electrolysis cell. The addition of Cl^- significantly improved the extent of phosphite oxidation because it was oxidized at the surface of the MMO anode to generate active chlorine (e.g., HClO, dissolved Cl_2; standard reduction potential of HClO/Cl^-: 1.49 V/SHE in acid medium),[13] which is also capable of oxidizing phosphite to phosphate. The elevated concentration of Cl^- from 0 to 150 mM yielded a faster rate of phosphite oxidation. Only 4.2% of phosphite was transformed to phosphate in the absence of Cl^-, and an almost 94% transformation was attained in the presence of 150 mM Cl^- within 150 min of treatment.

An interesting note was the distinctly enhanced transformation of phosphite to phosphate, as the Fe anode was introduced in the electrochemical reactor with a low applied current (10 mA). The presence of the Fe anode increased the rate of phosphate formation by 400.2% at 50 mM Cl^-. When 100 mM Cl^- was available in the electrolyte, the dual-anode system resulted in a 168.4% increase in the reaction rate compared with the single-anode system without the Fe anode. Almost 95% of phosphite was oxidized to phosphate at 100 mM Cl^- after 150 min of operation, and this value reached 100% at 150 mM Cl^- (less than 150 min of operation) in the

https://dx.doi.org/10.1021/acs.est.0c00218
Environ. Sci. Technol. 2020, 54, 6406−6414

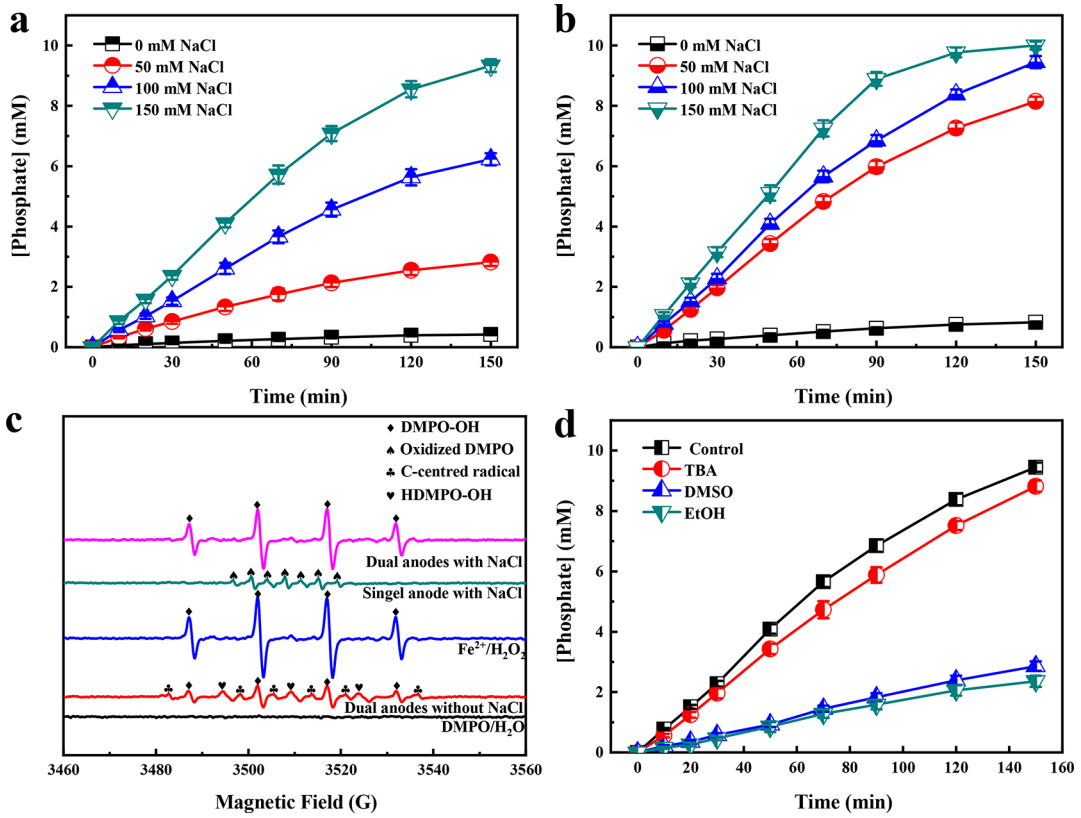

Figure 6. Time courses of phosphate concentrations as a function of time for different treatments: (a) single-anode (MMO) mode and (b) dual-anode (MMO/Fe) mode. I_{MMO} = 200 mA; I_{Fe} = 10 mA; [initial phosphite] = 10 mM; and initial pH = 2.2. (c) Comparisons of DMPO-probed ESR spectra of different systems under the conditions: [Fe^{2+}] = 200 μM; [H_2O_2] = 400 μM; $t_{electro}$ = 10 min; [NaCl] = 50 mM; [DMPO] = 100 mM; and initial pH = 2.2. (d) Time course of phosphate concentrations in the presence of different scavengers under the conditions: [initial phosphite] = 10 mM; [NaCl] = 100 mM; I_{MMO} = 200 mA, I_{Fe} = 10 mA; [scavengers] = 100 mM; and initial pH = 2.2.

dual-anode electrolytic system. It was also noticeable that the implantation of the Fe anode can improve phosphite oxidation in the absence of Cl^-. This can be explained by the fact that the reaction between in situ electrogenerated Fe^{2+} (from the Fe anode) and O_2 (from the MMO anode) results in the production of reactive oxygen species (ROS), such as $^{\bullet}O_2^-$ and $^{\bullet}OH$.[48] Nevertheless, only 8.2% transformation was obtained, which is much lower than the 81.5% in the same system containing 50 mM Cl^-, because the chain reactions for ROS generation are sluggish in acid medium.[49] It can thus be concluded that both Fe^{2+} and Cl^- available in the dual-anode electrochemical system play a critical role in accelerating phosphite oxidation owing to the presence of large amounts of $Fe^{IV}O^{2+}$ generated from the Fe^{2+}/HClO reaction.

Despite the importance of dissolved Fe^{2+} in improving the oxidizing capability of the system, excessive amounts of Fe^{2+} would impede phosphite transformation. For example (Figure S7a), when the current at the Fe anode was raised to 20 mA, favoring a greater extent of iron dissolution, the rate of phosphite oxidation dropped by 51.1%, compared with that associated with 10 mA applied to the Fe anode in the presence of 50 mM NaCl. Another example (Figure S7b) is that a one-time dose of 2.33 mM $FeCl_2$ (the amount is equal to the theoretically calculated value that dissolved from the Fe anode in 150 min) only led to 38.5% of phosphite being oxidized to phosphate, much less than the 81.5% obtained with the Fe anode (10 mA) that gradually released Fe^{2+}. This observation is likely the consequence of the reaction between excessive Fe^{2+} and the oxidative $Fe^{IV}O^{2+}$ to form Fe(III), an undesirable reaction that reduces the oxidative capacity of the electrochemical system.[50]

ESR and quenching experiments were also performed to verify the formation of $Fe^{IV}O^{2+}$ in the dual-anode electrochemical system that allows the in situ generation of Fe^{2+} and HClO. As shown in Figure 6c, the spectrum of the dual-anode system in the absence of Cl^- exhibited relatively weak signals, which are assigned to the DMPO−OH (with h_{fsc} of αN = αH = 14.9 G), HDMPO−OH (with h_{fsc} of αN = 14.6 G and αH = 1.1 G), and DMPO adducts of a carbon-centered radical (with h_{fsc} of αN = 15.4 G and αH = 22.3 G). This implies the presence of oxidative species, possibly $^{\bullet}O_2^-$ and $^{\bullet}OH$, which originated from the reaction between Fe^{2+} and O_2 generated in situ.[51] The ESR spectrum of the dual-anode system in the presence of 50 mM Cl^- displayed much stronger peaks corresponding to the DMPO−OH adducts, which is exactly consistent with the ESR spectrum of the Fe^{2+} and HClO system shown in Figure 4. Note that in the spectrum of the single-anode system (without the Fe anode), only signals related to the direct oxidation of DMPO were observed, implying the vital role of Fe^{2+} for reactive species formation in this electrochemical system. To clarify the involvement of $Fe^{IV}O^{2+}$ in the appearance of DMPO−OH adducts and the oxidation of phosphite in the dual-anode electrochemical reactor, scavenging experiments were undertaken using TBA[41] to quench $^{\bullet}OH$ and ethanol alcohol (EtOH)[7]/DMSO[6] to deactivate $Fe^{IV}O^{2+}$. As Figure 6d illustrates, the introduction of TBA to the system had an insignificant impact on phosphite oxidation, with only a 6.6% decrease in the amount of

https://dx.doi.org/10.1021/acs.est.0c00218
Environ. Sci. Technol. 2020, 54, 6406−6414

phosphate formed. However, the addition of EtOH and DMSO substantially suppressed the amount of phosphite oxidized, decreasing it by 68.5 and 72.9%, respectively. This comparison proves that $Fe^{IV}O^{2+}$ rather than $^{\bullet}OH$ is the pivotal in situ-generated reactive species for the acceleration of phosphite oxidation.

Environmental Implications. We have provided multiple lines of evidence to identify the generation of $Fe^{IV}O^{2+}$ rather than $^{\bullet}OH$ from the reaction between Fe^{2+} and HClO in an acid medium, offering insights into the radical and nonradical chemistry of the Fe(II)-mediated redox system. The evidence includes the results from XANES examinations, Mössbauer spectroscopic tests, PMSO-based probe experiments, ESR characterizations, and DFT calculations, all of which coincidently support the finding. We have also constructed a dual-anode electrolytic cell for the in situ generation of Fe^{2+} and HClO in order to demonstrate the $Fe^{IV}O^{2+}$-enhanced AOPs for the oxidation of an aqueous pollutant (e.g., phosphite), as depicted in Figure S8.

Despite the lower oxidizing potential of $Fe^{IV}O^{2+}$ (the standard redox potential of $Fe^{IV}O^{2+}/Fe^{3+}$ is 2.0 V vs SHE) compared with $^{\bullet}OH$ (the standard redox potential of $^{\bullet}OH/H_2O$ is 2.8 V vs SHE),[48] $Fe^{IV}O^{2+}$ as an electropositive species is advantageous because of its high selectivity and reasonable activity for the oxidation of pollutants.[8] This is important because nonselective radicals such as $^{\bullet}OH$ can react with coexisting substances, such as natural organic matter, halides, and carbonates, available in real wastewater.[48] These competitive reactions are susceptible to reducing the rate of removal of target pollutants. The established system in this study for $Fe^{IV}O^{2+}$ generation should represent an excellent platform for further in-depth investigation of its oxidation selectivity toward different contaminants.

Furthermore, in recent years, the idea of using the iron-based electrocoagulation/electro-oxidation (EC/EO) system with dual anodes for oxidizing various inorganic and organic compounds has aroused scientific and technological interest. The generation of oxidative intermediates such as Fe(IV), $^{\bullet}OH$, and $^{\bullet}O_2^-$ from the reaction between Fe(II) and O_2 (both species are generated in situ in the system) has been demonstrated.[21,48,52] However, few studies have addressed the contribution of the Fe(II)/active chlorine system to pollutant oxidation. (Active chlorine is an inevitable by-product of EO in Cl^--containing media.) The discovery of $Fe^{IV}O^{2+}$in the iron-involved EC/EO system that is used for treating Cl^--containing water represents a significant preoxidation step for the removal of some pollutants (e.g., phosphite, arsenite, and heavy metal−organic complexes). This leads to the production of their relevant compounds in the oxidized state, compounds that are more conducive to coagulation.[21,52] In the future, based on the established dual-anode electrochemical setup (Figure S8), we will endeavor to further explore the extent of $Fe^{(IV)}O^{2+}$ generation in real wastewater laden with Cl^- and how $Fe^{(IV)}O^{2+}$ generation contributes to the transformation of target contaminants with desirable products.

■ ASSOCIATED CONTENT

Supporting Information

The Supporting Information is available free of charge at https://pubs.acs.org/doi/10.1021/acs.est.0c00218.

Fe *K*-edge XANES; ESI-QqQMS measurements; ESR tests; DFT calculations on the Fe^{2+}/HClO reaction thermodynamics; and in situ generation of Fe^{2+} and HClO in a dual-anode electrochemical system and its application in the acceleration of phosphite oxidation (PDF)

■ AUTHOR INFORMATION

Corresponding Authors

Chengshuai Liu − *Guangdong Key Laboratory of Agricultural Environment Pollution Integrated Control, Guangdong Institute of Eco-Environmental and Soil Sciences, Guangzhou 510640, PR China; State Key Laboratory of Environmental Geochemistry, Institute of Geochemistry, Chinese Academy of Sciences, Guiyang 550081, PR China*; Email: csliu@soil.gd.cn

Chunhua Feng − *The Key Lab of Pollution Control and Ecosystem Restoration in Industry Clusters, Ministry of Education, School of Environment and Energy, South China University of Technology, Guangzhou 510006, PR China*; orcid.org/0000-0001-7928-7865; Email: chfeng@scut.edu.cn

Authors

Sheng Liang − *The Key Lab of Pollution Control and Ecosystem Restoration in Industry Clusters, Ministry of Education, School of Environment and Energy, South China University of Technology, Guangzhou 510006, PR China*

Liuyi Zhu − *The Key Lab of Pollution Control and Ecosystem Restoration in Industry Clusters, Ministry of Education, School of Environment and Energy, South China University of Technology, Guangzhou 510006, PR China*

Jian Hua − *Guangdong Key Laboratory of Agricultural Environment Pollution Integrated Control, Guangdong Institute of Eco-Environmental and Soil Sciences, Guangzhou 510640, PR China*

Weijian Duan − *The Key Lab of Pollution Control and Ecosystem Restoration in Industry Clusters, Ministry of Education, School of Environment and Energy, South China University of Technology, Guangzhou 510006, PR China*

Puu-Tai Yang − *Department of Agricultural Chemistry, National Taiwan University, Taipei 10617, Taiwan, ROC*

Shan-Li Wang − *Department of Agricultural Chemistry, National Taiwan University, Taipei 10617, Taiwan, ROC*; orcid.org/0000-0003-3156-5365

Chaohai Wei − *The Key Lab of Pollution Control and Ecosystem Restoration in Industry Clusters, Ministry of Education, School of Environment and Energy, South China University of Technology, Guangzhou 510006, PR China*

Complete contact information is available at: https://pubs.acs.org/10.1021/acs.est.0c00218

Author Contributions

The manuscript was written with contributions from all authors. All authors have approved the final version of the manuscript.

Notes

The authors declare no competing financial interest.

■ ACKNOWLEDGMENTS

We gratefully acknowledge financial support from the National Natural Science Foundation of China (nos. 21876052 and 21577041), the Science and Technology Program of Guangzhou, China (no. 201904010293 and 201704020200), and the Science and Technology Planning Project of

Guangdong Province, China (nos. 2019A050510009 and 2016TX03Z086). We also thank the National Synchrotron Radiation Research Center, Hsinchu, Taiwan, for providing XAS beamtime.

REFERENCES

(1) Fenton, H. J. H. LXXIII.—Oxidation of tartaric acid in presence of iron. *J. Chem. Soc., Trans.* **1894**, *65*, 899−910.
(2) Barb, W. G.; Baxendale, J. H.; George, P.; Hargrave, K. R. Reactions of ferrous and ferric ions with hydrogen peroxide. *Nature* **1949**, *163*, 692−694.
(3) Gligorovski, S.; Strekowski, R.; Barbati, S.; Vione, D. Environmental implications of hydroxyl radicals (•OH). *Chem. Rev.* **2015**, *115*, 13051−13092.
(4) Sun, M.; Chu, C.; Geng, F.; Lu, X.; Qu, J.; Crittenden, J.; Elimelech, M.; Kim, J.-H. Reinventing Fenton chemistry: Iron oxychloride nanosheet for pH-insensitive H_2O_2 activation. *Environ. Sci. Technol. Lett.* **2018**, *5*, 186−191.
(5) Cheaib, K.; Mubarak, M. Q. E.; Sénéchal-David, K.; Herrero, C.; Guillot, R.; Clémancey, M.; Latour, J.-M.; de Visser, S. P.; Mahy, J.-P.; Banse, F.; Avenier, F. Selective formation of an FeIVO or an FeIIIOOH intermediate from iron(II) and H_2O_2: Controlled heterolytic versus homolytic oxygen−oxygen bond cleavage by the second coordination sphere. *Angew. Chem.* **2019**, *131*, 864−868.
(6) Bataineh, H.; Pestovsky, O.; Bakac, A. pH-induced mechanistic changeover from hydroxyl radicals to iron(iv) in the Fenton reaction. *Chem. Sci.* **2012**, *3*, 1594−1599.
(7) Wang, Z.; Jiang, J.; Pang, S.; Zhou, Y.; Guan, C.; Gao, Y.; Li, J.; Yang, Y.; Qiu, W.; Jiang, C. Is sulfate radical really generated from peroxydisulfate activated by iron(II) for environmental decontamination? *Environ. Sci. Technol.* **2018**, *52*, 11276−11284.
(8) Li, H.; Shan, C.; Li, W.; Pan, B. Peroxymonosulfate activation by iron(III)-tetraamidomacrocyclic ligand for degradation of organic pollutants via high-valent iron-oxo complex. *Water Res.* **2018**, *147*, 233−241.
(9) Kim, J.; Zhang, T.; Liu, W.; Du, P.; Dobson, J. T.; Huang, C.-H. Advanced oxidation process with peracetic acid and Fe(II) for contaminant degradation. *Environ. Sci. Technol.* **2019**, *53*, 13312−13322.
(10) Dong, H.; Li, Y.; Wang, S.; Liu, W.; Zhou, G.; Xie, Y.; Guan, X. Both Fe(IV) and radicals are active oxidants in the Fe(II)/peroxydisulfate process. *Environ. Sci. Technol. Lett.* **2020**, *7*, 219.
(11) Nowicka, A. M.; Hasse, U.; Hermes, M.; Scholz, F. Hydroxyl radicals attack metallic gold. *Angew. Chem., Int. Ed.* **2010**, *49*, 1061−1063.
(12) Kishimoto, N.; Kitamura, T.; Kato, M.; Otsu, H. Reusability of iron sludge as an iron source for the electrochemical Fenton-type process using Fe^{2+}/HOCl system. *Water Res.* **2013**, *47*, 1919−1927.
(13) Aguilar, Z. G.; Brillas, E.; Salazar, M.; Nava, J. L.; Sirés, I. Evidence of Fenton-like reaction with active chlorine during the electrocatalytic oxidation of acid yellow 36 azo dye with Ir-Sn-Sb oxide anode in the presence of iron ion. *Appl. Catal., B* **2017**, *206*, 44−52.
(14) Kishimoto, N.; Nakamura, Y.; Kato, M.; Otsu, H. Effect of oxidation−reduction potential on an electrochemical Fenton-type process. *Chem. Eng. J.* **2015**, *260*, 590−595.
(15) Conocchioli, T. J.; Hamilton, E. J.; Sutin, N. The formation of iron(IV) in the oxidation of iron(II)[1]. *J. Am. Chem. Soc.* **1965**, *87*, 926−927.
(16) Pestovsky, O.; Bakac, A. Aqueous ferryl(IV) ion: Kinetics of oxygen atom transfer to substrates and oxo exchange with solvent water. *Inorg. Chem.* **2006**, *45*, 814−820.
(17) Martinho, M.; Banse, F.; Bartoli, J.-F.; Mattioli, T. A.; Battioni, P.; Horner, O.; Bourcier, S.; Girerd, J.-J. New example of a non-heme mononuclear iron(IV) oxo complex. Spectroscopic data and oxidation activity. *Inorg. Chem.* **2005**, *44*, 9592−9596.
(18) Rohde, J.-U.; Lim, M. H.; Brennessel, W. W.; Bukowski, M. R.; Stubna, A.; Münck, E.; Nam, W.; Que, L. Crystallographic and spectroscopic characterization of a nonheme Fe(IV)=O complex. *Science* **2003**, *299*, 1037−1039.
(19) Nam, W. High-valent iron(IV)−oxo complexes of heme and non-heme ligands in oxygenation reactions. *Acc. Chem. Res.* **2007**, *40*, 522−531.
(20) Pestovsky, O.; Stoian, S.; Bominaar, E. L.; Shan, X.; Münck, E.; Que, L., Jr.; Bakac, A. Aqueous FeIV=O: Spectroscopic identification and oxo-group exchange. *Angew. Chem., Int. Ed.* **2005**, *44*, 6871−6874.
(21) Liang, S.; Zheng, W.; Zhu, L.; Duan, W.; Wei, C.; Feng, C. One-step treatment of phosphite-laden wastewater: A single electrochemical reactor integrating superoxide radical-induced oxidation and electrocoagulation. *Environ. Sci. Technol.* **2019**, *53*, 5328−5336.
(22) Cai, Z.; Zhou, D.; Wang, M.; Bak, S.-M.; Wu, Y.; Wu, Z.; Tian, Y.; Xiong, X.; Li, Y.; Liu, W.; Siahrostami, S.; Kuang, Y.; Yang, X.-Q.; Duan, H.; Feng, Z.; Wang, H.; Sun, X. Introducing Fe(2+) into nickel-iron layered double hydroxide: Local structure modulated water oxidation activity. *Angew. Chem.* **2018**, *57*, 9392−9396.
(23) Haas, O.; Vogt, U. F.; Soltmann, C.; Braun, A.; Yoon, W.-S.; Yang, X. Q.; Graule, T. The Fe K-edge X-ray absorption characteristics of La1-xSrxFeO3-δ prepared by solid state reaction. *Mater. Res. Bull.* **2009**, *44*, 1397−1404.
(24) Friebel, D.; Louie, M. W.; Bajdich, M.; Sanwald, K. E.; Cai, Y.; Wise, A. M.; Cheng, M.-J.; Sokaras, D.; Weng, T.-C.; Alonso-Mori, R.; Davis, R. C.; Bargar, J. R.; Nørskov, J. K.; Nilsson, A.; Bell, A. T. Identification of highly active Fe sites in (Ni,Fe)OOH for electrocatalytic water splitting. *J. Am. Chem. Soc.* **2015**, *137*, 1305−1313.
(25) Mills, M. R.; Weitz, A. C.; Hendrich, M. P.; Ryabov, A. D.; Collins, T. J. NaClO-generated iron(IV)oxo and iron(V)oxo TAMLs in pure water. *J. Am. Chem. Soc.* **2016**, *138*, 13866−13869.
(26) Mártire, D. O.; Caregnato, P.; Furlong, J.; Allegretti, P.; Gonzalez, M. C. Kinetic study of the reactions of oxoiron(IV) with aromatic substrates in aqueous solutions. *Int. J. Chem. Kinet.* **2002**, *34*, 488−494.
(27) Shao, B.; Dong, H.; Sun, B.; Guan, X. Role of ferrate(IV) and ferrate(V) in activating ferrate(VI) by calcium sulfite for enhanced oxidation of organic contaminants. *Environ. Sci. Technol.* **2019**, *53*, 894−902.
(28) Pascualini, M. E.; Di Russo, N. V.; Thuijs, A. E.; Ozarowski, A.; Stoian, S. A.; Abboud, K. A.; Christou, G.; Veige, A. S. A high-spin square-planar Fe(ii) complex stabilized by a trianionic pincer-type ligand and conclusive evidence for retention of geometry and spin state in solution. *Chem. Sci.* **2015**, *6*, 608−612.
(29) Hoffart, L. M.; Barr, E. W.; Guyer, R. B.; Bollinger, J. M.; Krebs, C. Direct spectroscopic detection of a C-H-cleaving high-spin Fe(IV) complex in a prolyl-4-hydroxylase. *Proc. Natl. Acad. Sci. U.S.A.* **2006**, *103*, 14738.
(30) Chen, J. Y. C.; Dang, L.; Liang, H.; Bi, W.; Gerken, J. B.; Jin, S.; Alp, E. E.; Stahl, S. S. Operando analysis of NiFe and Fe oxyhydroxide electrocatalysts for water oxidation: Detection of Fe^{4+} by mössbauer spectroscopy. *J. Am. Chem. Soc.* **2015**, *137*, 15090−15093.
(31) Gupta, R.; Lacy, D. C.; Bominaar, E. L.; Borovik, A. S.; Hendrich, M. P. Electron paramagnetic resonance and mössbauer spectroscopy and density functional theory analysis of a high-spin FeIV−oxo complex. *J. Am. Chem. Soc.* **2012**, *134*, 9775−9784.
(32) Krebs, C.; Price, J. C.; Baldwin, J.; Saleh, L.; Green, M. T.; Bollinger, J. M. Rapid freeze-quench 57Fe mössbauer spectroscopy: Monitoring changes of an iron-containing active site during a biochemical reaction. *Inorg. Chem.* **2005**, *44*, 742−757.
(33) Neese, F. Theoretical spectroscopy of model-nonheme $[Fe(IV)OL_5]^{2+}$ complexes in their lowest triplet and quintet states using multireference ab initio and density functional theory methods. *J. Inorg. Biochem.* **2006**, *100*, 716−726.
(34) Pestovsky, O.; Bakac, A. Reactivity of aqueous Fe(IV) in hydride and hydrogen atom transfer reactions. *J. Am. Chem. Soc.* **2004**, *126*, 13757−13764.
(35) Pang, S.-Y.; Jiang, J.; Ma, J. Oxidation of sulfoxides and arsenic(III) in corrosion of nanoscale zero valent iron by oxygen:

https://dx.doi.org/10.1021/acs.est.0c00218
Environ. Sci. Technol. 2020, 54, 6406−6414

Evidence against ferryl ions (Fe(IV)) as active intermediates in Fenton reaction. *Environ. Sci. Technol.* **2011**, *45*, 307−312.
(36) Feng, G.; Cheng, P.; Yan, W.; Boronat, M.; Li, X.; Su, J.-H.; Wang, J.; Li, Y.; Corma, A.; Xu, R.; Yu, J. Accelerated crystallization of zeolites via hydroxyl free radicals. *Science* **2016**, *351*, 1188.
(37) Makino, K.; Hagiwara, T.; Hagi, A.; Nishi, M.; Murakami, A. Cautionary note for DMPO spin trapping in the presence of iron ion. *Biochem. Biophys. Res. Commun.* **1990**, *172*, 1073−1080.
(38) Burkitt, M. J.; Ying Tsang, S.; Ching Tam, S.; Bremner, I. Generation of 5,5-dimethyl-1-pyrrolineN-oxide hydroxyl and scavenger radical adducts from copper/H_2O_2 mixtures: Effects of metal ion chelation and the search for high-valent metal−oxygen intermediates. *Arch. Biochem. Biophys.* **1995**, *323*, 63−70.
(39) Xu, K.; Ben, W.; Ling, W.; Zhang, Y.; Qu, J.; Qiang, Z. Impact of humic acid on the degradation of levofloxacin by aqueous permanganate: Kinetics and mechanism. *Water Res.* **2017**, *123*, 67−74.
(40) Yang, Z.; Qian, J.; Yu, A.; Pan, B. Singlet oxygen mediated iron-based Fenton-like catalysis under nanoconfinement. *Proc. Natl. Acad. Sci. U.S.A.* **2019**, *116*, 6659.
(41) Yamazaki, I.; Piette, L. H. EPR spin-trapping study on the oxidizing species formed in the reaction of the ferrous ion with hydrogen peroxide. *J. Am. Chem. Soc.* **1991**, *113*, 7588−7593.
(42) Candeias, L. P.; Stratford, M. R. L.; Wardman, P. Formation of hydroxyl radicals on reaction of hypochlorous acid with ferrocyanide, a model iron(II) complex. *Free Radical Res.* **1994**, *20*, 241−249.
(43) Coledam, D. A. C.; Sánchez-Montes, I.; Silva, B. F.; Aquino, J. M. On the performance of HOCl/Fe^{2+}, HOCl/Fe^{2+}/UVA, and HOCl/UVC processes using in situ electrogenerated active chlorine to mineralize the herbicide picloram. *Appl. Catal., B* **2018**, *227*, 170−177.
(44) Buda, F.; Ensing, B.; Gribnau, M. C. M.; Baerends, E. J. DFT study of the active intermediate in the Fenton reaction. *Chem.—Eur. J.* **2001**, *7*, 2775−2783.
(45) Miertuš, S.; Tomasi, J. Approximate evaluations of the electrostatic free energy and internal energy changes in solution processes. *Chem. Phys.* **1982**, *65*, 239−245.
(46) Cantú Reinhard, F. G.; Faponle, A. S.; de Visser, S. P. Substrate sulfoxidation by an iron(IV)-oxo complex: Benchmarking computationally calculated barrier heights to experiment. *J. Phys. Chem. A* **2016**, *120*, 9805−9814.
(47) Yang, T.; Quesne, M. G.; Neu, H. M.; Cantú Reinhard, F. G.; Goldberg, D. P.; de Visser, S. P. Singlet versus triplet reactivity in an Mn(V)−oxo species: Testing theoretical predictions against experimental evidence. *J. Am. Chem. Soc.* **2016**, *138*, 12375−12386.
(48) Qian, A.; Yuan, S.; Xie, S.; Tong, M.; Zhang, P.; Zheng, Y. Oxidizing capacity of iron electrocoagulation systems for refractory organic contaminant transformation. *Environ. Sci. Technol.* **2019**, *53*, 12629−12638.
(49) Lakshmanan, D.; Clifford, D. A.; Samanta, G. Ferrous and ferric ion generation during iron electrocoagulation. *Environ. Sci. Technol.* **2009**, *43*, 3853−3859.
(50) Li, L.; van Genuchten, C. M.; Addy, S. E. A.; Yao, J.; Gao, N.; Gadgil, A. J. Modeling As(III) oxidation and removal with iron electrocoagulation in groundwater. *Environ. Sci. Technol.* **2012**, *46*, 12038−12045.
(51) Cui, J.; Wang, X.; Zhang, J.; Qiu, X.; Wang, D.; Zhao, Y.; Xi, B.; Alshawabkeh, A. N.; Mao, X. Disilicate-assisted iron electrolysis for sequential Fenton-oxidation and coagulation of aqueous contaminants. *Environ. Sci. Technol.* **2017**, *51*, 8077−8084.
(52) Tong, M.; Yuan, S.; Zhang, P.; Liao, P.; Alshawabkeh, A. N.; Xie, X.; Wang, Y. Electrochemically induced oxidative precipitation of Fe(II) for As(III) oxidation and removal in synthetic groundwater. *Environ. Sci. Technol.* **2014**, *48*, 5145−5153.

https://dx.doi.org/10.1021/acs.est.0c00218
Environ. Sci. Technol. 2020, 54, 6406−6414